

# Effect of biaxial stress state on seismic fragility of concrete gravity dams

Ufuk Sen<sup>1a</sup> and Ayman M. Okeil<sup>\*2</sup>

<sup>1</sup>General Directorate of State Hydraulic Works, Turkey

<sup>2</sup>Department of Civil and Environmental Engineering, Louisiana State University, Baton Rouge, Louisiana, USA

(Received February 22, 2019, Revised September 11, 2019, Accepted December 26, 2019)

**Abstract.** Dams are important structures for management of water supply for irrigation or drinking, flood control, and electricity generation. In seismic regions, the structural safety of concrete gravity dams is important due to the high potential of life and economic loss if they fail. Therefore, the seismic analysis of existing dams in seismically active regions is crucial for predicting responses of dams to ground motions. In this paper, earthquake response of concrete gravity dams is investigated using the finite element (FE) method. The FE model accounts for dam-water-foundation rock interaction by considering compressible water, flexible foundation effects, and absorptive reservoir bottom materials. Several uncertainties regarding structural attributes of the dam and external actions are considered to obtain the fragility curves of the dam-water-foundation rock system. The structural uncertainties are sampled using the Latin Hypercube Sampling method. The Pine Flat Dam in the Central Valley of Fresno County, California, is selected to demonstrate the methodology for several limit states. The fragility curves for base sliding, and excessive deformation limit states are obtained by performing non-linear time history analyses. Tensile cracking including the complex state of stress that occurs in dams was also considered. Normal, Log-Normal and Weibull distribution types are considered as possible fits for fragility curves. It was found that the effect of the minimum principal stress on tensile strength is insignificant. It is also found that the probability of failure of tensile cracking is higher than that for base sliding of the dam. Furthermore, the loss of reservoir control is unlikely for a moderate earthquake.

**Keywords:** concrete gravity dams; fragility; safety; reliability; probability; earthquake engineering

## 1. Introduction

Dams are important structures for management of water supply for irrigation or drinking, flood control, and electricity generation. The safety analysis of concrete gravity dams in seismic regions is important due to the high potential of life and economic losses if they fail. Many existing dams were built using outdated analysis methods and limited understanding of seismicity (Bernier *et al.* 2016). In the design of many existing dams, dam-water-foundation interactions are known to affect the earthquake response, yet they were not considered due to the lack of knowledge or computational resources. The American Society of Civil Engineers (ASCE) estimates that out of 90,580 dams in the US, 15,498 (17.12%) dams have high potential risk of causing loss of life, and 11,882 (13.12%) dams are in the category of causing significant economic losses (ASCE 2017). Therefore, the seismic analysis of existing dams in seismically active regions is crucial to predict responses of dams to ground motions. Dams are usually analyzed using deterministic analysis methods. However, several uncertainties affecting the results, such as material properties, modeling inaccuracies, the water level in the reservoir, and the aleatoric nature of earthquakes,

should be considered in the analyses of the dams (Lupoi and Callari 2011).

To consider these uncertainties, the first probabilistic seismic analysis of concrete gravity dams was carried out by de Araujo and Awruch (1998). Random material properties and seismic excitation were considered in the analyses. The fragility curves for different limit states are obtained using the Monte Carlo Simulation (MCS) method. Tekie and Ellingwood (2003) presented a methodology to obtain fragility curves of concrete gravity dams by considering both material and seismic uncertainties using Latin Hypercube sampling (LHS) to handle the effect of uncertainties. Another probabilistic method was presented by Lupoi and Callari (2011). The water level was also considered as a random as well as material and seismic uncertainties and the MCS method was used to obtain fragility curves. Ghanaat *et al.* (2012) also studied the seismic fragility analysis of concrete gravity dams considering the sliding at the lift joint at the neck of the dam model as one of the limit states. Fragility curves were fitted using the Weibull cumulative distribution functions. Bernier *et al.* (2016) obtained the fragility curves for the base and neck sliding response of the concrete gravity dam. The spatial variation of the friction coefficient was included in the analyses. Also, it was found that the spatial variation of the angle of friction at dam-foundation rock interaction is not significant when the seismic intensity level is low. Despite the three-dimensional nature of concrete gravity dams, which produces complex stress states under seismic loads, a uniaxial failure envelope for concrete was assumed in assessing the cracking probability of failure in all the

\*Corresponding author, Professor  
E-mail: [aokeil@lsu.edu](mailto:aokeil@lsu.edu)

<sup>a</sup>Professor  
E-mail: [usen1@lsu.edu](mailto:usen1@lsu.edu)

studies that considered concrete cracking. The effect of the vertical component of the ground motion on fragility curves for concrete dams was investigated by Hariri-Ardebili and Saouma (2016a), and the obtained curves were compared with well-established ones for framed structures. In another paper, Hariri-Ardebili and Saouma (2016b) conducted a state-of-the-art review of published research on seismic fragility of concrete dams in which they concluded that nonlinearities deserve to be considered in future studies since linear analyses may only be suitable for serviceability investigations. Morales-Torres *et al.* (2016) presented a methodology for developing fragility curves for concrete gravity dams sliding failure considering natural and epistemic uncertainties. The developed framework addressed several issues that are often faced when developing fragility curves such as the handling of relevant variables and type of probability distribution and revealed that understanding the impact of epistemic uncertainty on the overall risk is important to improving dam safety.

In this paper, a methodology for developing the fragility curves for concrete gravity dams considering material and seismic uncertainties is presented. Four different failure modes, namely base sliding, concrete cracking at the base and neck of the upstream face, and excessive deformations, are taken into account. By considering different three threshold levels for base sliding and two for excessive deformations, the total number of limit states considered was seven. In previous studies, only the maximum principal stress is considered to evaluate the crack formation due to the tensile stress. However, in this study, in the calculations of the tensile strength capacity, the effect of the minimum principal stress, which affects concrete tensile strength, is considered. The Pine Flat Dam using Latin Hypercube Sampling method is chosen to demonstrate the developed methodology and discuss the obtained results. In addition, the number of analyses increased by matching each random model with 3 different ground motions to get more reliable results, which will be explained in more detail in Section 4.2.

Design and analysis models often idealize structures into simpler structures than they actually are. Consequently, structures are often subjected to complex states of stress than idealized design and analysis models can account for. This is done for the sake of simplifying the design process. The ignored stresses may contribute to undesirable effects that may lead to premature failure if they have a significant adverse effect on the structural capacity. Therefore, the effects of multiaxial state of stress should be investigated to assess their importance in the design process. In this study, the critical case of biaxial (tension-compression) state of stress is considered in the development of fragility curves for concrete gravity dams. It is known that orthogonal compressive stresses reduce the tensile capacity of concrete. This effect was accounted for by using the minimum principal stress corresponding to the critical tensile stress at critical locations in concrete gravity dams.

## 2. Fragility analysis

Fragility curves are important to dam owners and

authorities to make structural risk assessments. In the general form, the seismic fragility is defined as the conditional probability of failure, or exceedance, of a certain limit state at a given intensity measure such as earthquake spectral acceleration or peak ground acceleration. Several limit states (LS) affecting the system performance are assessed in a typical safety analysis of concrete gravity dams. In this paper, base sliding, cracking of the dam concrete due to tensile stress, and excessive deformation of the dam body are assessed as described in detail later. Each limit state probability can be expressed by (Ghanaat *et al.* 2012)

$$P(LS < 0) = \sum_y P(LS < 0|Y = y)P(Y = y) \quad (1)$$

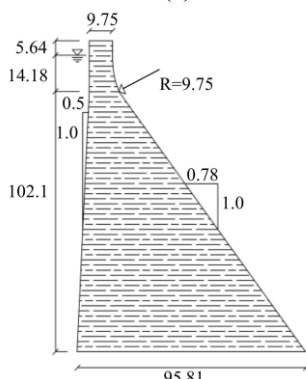
where  $Y$  is a random variable describing the intensity of demand,  $P(Y = y)$  is the (annual) probability of this demand, and  $P(LS < 0|Y = y)$  is the conditional probability of LS, given that  $Y = y$ . This conditional probability is defined as the ‘fragility’ (Ellingwood and Tekie 2001). The fragility curve is a plot of the probability that a structure would fail to perform satisfactorily when subjected to a range of intensities of a specific event. All uncertainties affecting the performance of the structure should be taken into account in the calculation of fragility. Uncertainties are usually divided into two groups: aleatory and epistemic uncertainties. **Aleatory Uncertainties** are produced by the inherent variability in the nature including the variability along time of an event or the variability across the space of an event or the variability of its magnitude (e.g., the variability in the intensity of ground motions). This kind of uncertainties cannot be reduced, but it can be estimated. **Epistemic Uncertainties** are the result of lack of knowledge arising from assumptions and limitations in the data. It also includes uncertainty due to inaccuracy of the model representing reality. An example of this kind of uncertainty can be the cohesion of the foundation rock. This kind of uncertainties can be reduced when the resources of the data are characterized better. Conducting fragility analysis for various structural systems and hazards have been gaining attention in recent years (Li *et al.* 2018, Moradloo *et al.* 2018, Nielson and DesRoches 2007, Salimi and Yazdani 2018).

## 3. Finite element model

In this paper, the Pine Flat Dam is selected as a case study in order to demonstrate the adopted methodology for developing fragility curves for concrete gravity dams by investigating its earthquake response. The dam is located in the Central Valley of Fresno County, California, and was commissioned in 1954. The highest non-overflow section is 121.92 m tall and the crest is 560.83 m long. The dam and its dimensions can be seen in Fig. 1. Table 1 lists the material properties of the dam, reservoir and foundation rock. The computer program ANSYS (2018) is used to model the dam-foundation-reservoir system. Two-dimensional PLANE42 are used to model the solid parts of the system; i.e., dam and foundation, and FLUID29



(a)



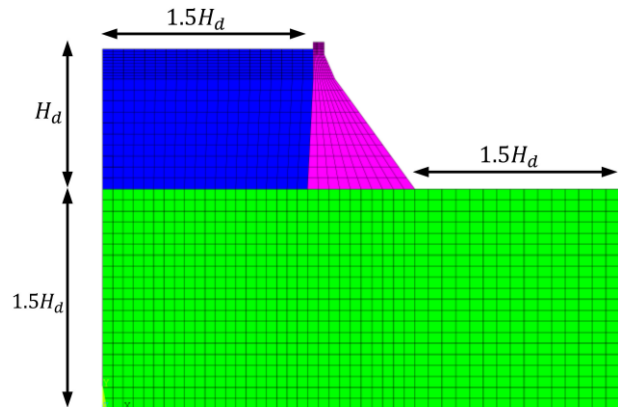
(b)

Fig. 1 View and dimensions (in meters) Pine Flat Dam

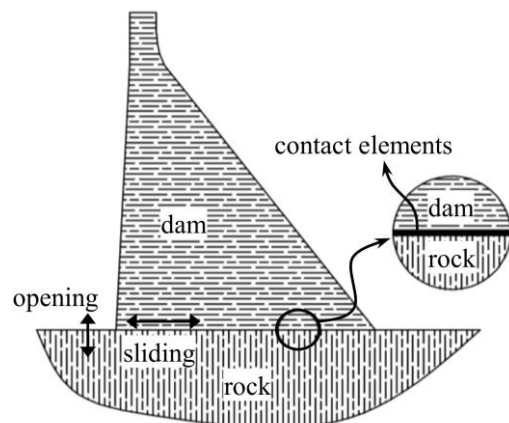
Table 1 Material properties of Pine Flat Dam (Fenves and Chopra 1984)

	Modulus of Elasticity (GPa)	Poisson's Ratio	Mass Density (kg/m <sup>3</sup> )	Sonic Velocity (m/s)	Wave Reflection Coefficient ( $\alpha$ )
Dam	22.4	0.20	2430	--	--
Foundation	22.4	0.33	2643	--	--
Reservoir	--	--	1000	1440	0.8

elements are used to model the fluid, i.e., reservoir. The PLANE42 element has four nodes with two degrees of freedom at each node, namely translation in  $x$  and  $y$  directions. The FLUID29 element has four nodes and each node has three degrees of freedom which are translations in  $x$  and  $y$  directions and pressure, however, the translation degrees of freedom are active only on the interface of fluid and structure. In order to decrease the effect of the FE model boundaries on the response of the system, the reservoir and foundation length, and foundation depth are selected 1.5 times longer than dam height. Zero pressure is applied at the truncated boundary of the reservoir to consider the damping effect arising from the propagation of pressure waves. In addition, zero pressure is applied at the top of reservoir by neglecting the effects of the surface waves, which are known to be small (Fenves and Chopra 1984). Finally, zero displacement is imposed on horizontal translation degrees of freedom at all boundaries of the foundation. However, only the translation degrees of freedom on the bottom boundary of the foundation was



(a)



(b)

Fig. 2 FE model of dam-reservoir-foundation rock system and contact interface

restrained in the vertical direction. The dam and foundation are assumed to be homogeneous, elastic and isotropic, and the fluid is assumed to be compressible and inviscid. Fig. 2(a) shows the FE model developed. The model consisted of 1140 PLANE42 elements for the dam and foundation rock and 400 FLUID29 elements for the reservoir.

### 3.1 Massless foundation

In the developed model, a massless foundation is assumed. Massless foundation modeling ignores the inertial effects of the foundation. Therefore, only the flexibility effects of the foundation are introduced into the system, which assists in preventing the propagation of artificial amplification of free-field ground motion. The massless foundation has zero damping, and this neglects the energy dissipation provided by the foundation. Therefore, the mathematical formulations for damping should be used in order to get more accurate results (Leger and Boughoufalah 1989). In this study, the following formulation provided by Fenves and Chopra (1987) was considered. It was recently found (Løkke and Chopra 2015) that using an individual viscous damping ratio for the dam alone and a separate viscous damping ratio for the foundation rock alone can cause excessive damping for the complete system. Therefore, this approach is not recommended for the

analysis of dam-water-foundation systems. The damping effect of the reservoir due to bottom materials such as sediments is also considered.

$$\tilde{\xi}_1 = \frac{1}{R_r} \frac{1}{(R_f)^3} \xi_1 + \xi_r + \xi_f \quad (2)$$

where  $R_r$  is the period lengthening ratio due to dam-water interaction;  $R_f$  is the period lengthening ratio due to dam-foundation interaction;  $\tilde{\xi}_1$  is damping ratio for dam on flexible foundation with impounded water;  $\xi_r$  is the added damping due to dam-water interaction;  $\xi_f$  is the added damping due to dam-foundation interaction;  $\xi_1$  is the damping ratio of dam on rigid foundation with empty reservoir. In this study, 5% damping ratio ( $\xi_1$ ) is assumed for the concrete dam. Other parameters in Eq. (2) were obtained from the tables in (Løkke and Chopra 2015).

The Rayleigh damping coefficients  $\alpha$  and  $\beta$ , which are the mass proportional damping and the stiffness proportional damping, respectively, are applied to the system. The following formulas are used in the calculation of these coefficients (Goldgruber *et al.* 2015)

$$\alpha = \xi \frac{2\omega_i\omega_j}{\omega_i + \omega_j} \quad (3a)$$

$$\beta = \xi \frac{2}{\omega_i + \omega_j} \quad (3b)$$

where  $\omega_i$  and  $\omega_j$  are the  $i^{th}$  and  $j^{th}$  fundamental frequencies of the dam-water-foundation system. In this study, the first and the fifth fundamental frequencies, which are 2.02 and 5.52 Hz, respectively, are used to calculate Rayleigh damping coefficients.

The self-weight of the dam is considered by adding 9.81 m/s<sup>2</sup> acceleration in the vertical direction while turning off the transient effects at the beginning of the time history analysis. The self-weight was kept applied during the earthquake analysis. In other words, the self-weight of the dam was considered as an initial condition to the time history analysis.

### 3.2 Dam-foundation interface modeling

Contour plots of the preliminary linear analysis show that the high tensile stresses at the base of the dam are around 3.04 MPa for an earthquake with 0.18g peak ground acceleration. This value exceeds the dam's concrete tensile strength which is 2.57 MPa for the given compressive strength of 22.43 MPa. Therefore, this stress level can cause cracking and sliding of the dam base. It also implies that adhesion between the dam and the foundation should be capable of resisting these high stress levels, which is unlikely. In order to model the separation that can happen between the dam and its supporting foundation, contact elements are modeled along the dam-foundation interface based on Coulomb-Mohr friction law using CONTA171 and TARGE169 elements in ANSYS. In the model, the contacting surfaces are capable of bearing shear stress up to a certain limit,  $\tau_{lim}$ , of shear stresses before they start to slide relative to each other. The shear stress capacity is

defined as follows

$$\tau_{lim}(t) = \sigma_n(t) \tan(\varphi) + c \quad (4)$$

where  $\tau_{lim}(t)$  and  $\sigma_n(t)$  are the shear capacity and the normal stress at time  $t$ , respectively, and  $\varphi$  is the friction angle, and  $c$  is the cohesion of the dam-foundation rock interface. Once the shear stress exceeds this capacity, the sliding of surfaces occurs.

The behavior of contact surface in the normal direction allows the contacting surfaces to transmit normal pressure before an opening occurs. In other words, these contact elements are able to transmit normal compressive stress, however, they will begin to open when the tensile stress is higher than the tensile strength. Opening and sliding behavior directions and where these contact elements are defined are shown in Fig. 2(b).

### 3.3 Ground motion

The ground motion acceleration was applied using the ACEL command in ANSYS, which combines the input acceleration with the element mass matrices to form a body force load vector, resulting in identical results to those obtained by applying acceleration from the bottom nodes of the model. When the acceleration is applied from the bottom nodes of the model, the relative displacement between the dam nodes and the bottom nodes should be considered as the nodes where the acceleration is applied experience displacements corresponding to the entered acceleration record. The absence of the foundation mass prevents propagation of artificial amplification of free-field ground motion.

### 3.4 Model validation

The tallest, non-overflow section shown in Fig. 1 was used to validate the developed FE model. The Kern County, California, earthquake of 21 July 1952 recorded at Taft Lincoln School Tunnel is selected to compare the results obtained from the developed FE model with Analysis results published by Fenves and Chopra (1984) for the Pine Flat Dam. The time history response was in excellent agreement with the published results. The horizontal and vertical displacement-time history graphs for the dam crest are presented in the Fig. 3. More information about the validation results can be found elsewhere (Sen 2018).

## 4. Reliability analysis

Uncertainties can have a significant effect on the evaluation of the performance of structures. This is especially true in seismic evaluations of structures due to random nature of earthquakes hazards and the uniqueness of each event. In the reliability analysis of concrete gravity dams, the sources of uncertainties are material properties, dimensions of the structure, and ground motion as well as water level. In this study, the uncertainties related to earthquakes and material properties are taken into account while considering the full reservoir case.

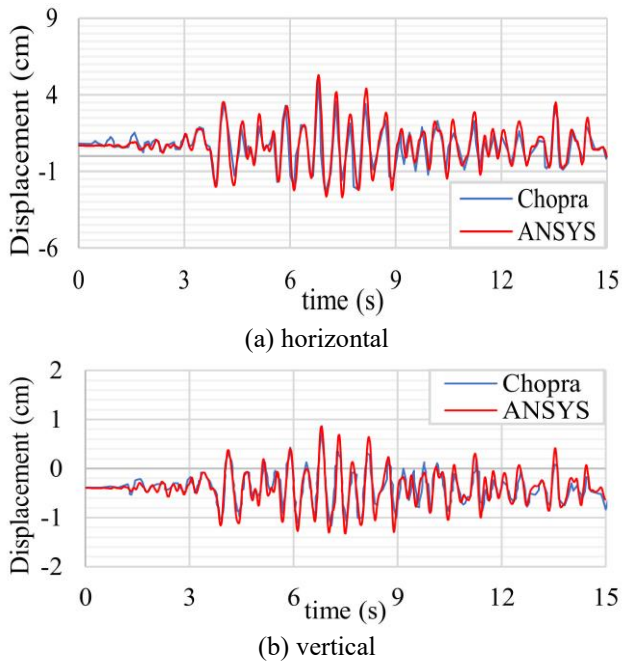


Fig. 3 Displacement time histories of the dam crest

Table 2 Random variables

Random Variable	Distribution Type	Distribution Parameters	
Cohesion (MPa)	Uniform	L = 0.3	Uniform
Friction Angle (°)	Uniform	L = 35	Uniform
Drain Efficiency (%)	Uniform	L = 0	Uniform
Rock Elasticity Modulus (GPa)	Uniform	L = 15.6	Uniform
Concrete Elasticity Modulus (GPa)	Normal	$\mu = 22.4$	Normal
Concrete Compressive Strength (MPa)	Log-Normal	$\mu = 22.43$	Log-Normal
Damping Coefficient $\alpha$	Uniform	L = 1.7133	Uniform
Damping Coefficient $\beta$	Uniform	L = 0.00325	Uniform

#### 4.1 Random variables

Table 2 lists the parameters considered as random variables in this study. Because of the scarcity of statistical info about some of these variables, a uniform distribution was assumed. Table 3 lists the twelve random variates for these variables that were considered in this study.

The cohesion and friction angle of the interface were chosen based on the Geologic Strength Index (GSI) of foundation rock considering elasticity modulus in order to use consistent parameters in the analyses. Therefore, GSI index derived from Eq. (5) for  $E_f=22.4$  GPa was determined to be equal to 64. The recommended cohesion and friction angle values for GSI 55 - 75 values are presented are GSI=55 - 75, Cohesion=0.3 - 0.4 MPa, and Friction Angle=35 - 45° (Hoek and Brown 1997).

$$E_f = 10^{(GSI-10)/40} \quad (\text{in GPa}) \quad (5)$$

Damping was also considered as a random variable. A

damping ratio equal to 9.8% was calculated for overall dam-reservoir-foundation rock system based on Eq. (2). The corresponding Rayleigh damping coefficients  $\alpha$  and  $\beta$  are calculated as 1.9037 and 0.00361, respectively, using Eq. (3). The distribution type and the range of the coefficient values are shown in Table 2.

Since it cannot be assumed that the concrete's elasticity modulus and compressive strength are independent random variables, the correlation between them was considered. In order to use consistent compressive strength with the elasticity modulus, Eq. (6) provided by ACI Committee (ACI 2014) is used. Therefore, for a nominal compressive strength equal to 22.43 MPa, the nominal elasticity modulus was taken equal to 22.4 GPa. The coefficient of variation value used in this study is 10% obtained from the literature (Nowak and Szerszen 2003). The correlation coefficient is assumed to be 0.8 between the concrete's elasticity modulus and compressive strength. The distribution type for the elasticity modulus and the compressive strength of concrete was assumed to be normal and lognormal, respectively, and the statistical parameters are shown in Table 2.

$$E_c = 4730\sqrt{f'_c} \quad , \quad \text{for } f'_c \leq 41.4 \text{ MPa and} \quad (6)$$

$$1440 \leq \gamma_c \leq 2480 \text{ kg/m}^3 \text{ (in GPa)}$$

The uplift pressure at the base of the dam due to the pore water is also randomized assuming a triangular distribution. The maximum uncertainty is considered by assuming uniform distribution between 0 - 100% drain efficiency due to the lack of knowledge about the drain system of the Pine Flat Dam, and drain line positions for 0% and 100% efficiency of drains are presented in Fig. 4. As stated in the US Army Corps of Engineers' report (USACE 1995), the pressure distribution due to pore water is considered unchanged during an earthquake.

#### 4.2 Sampling method

Some researchers state that the minimum number of simulations for providing reliable results to obtain fragility curves is 10 (Ghanaat *et al.* 2012). In this study, twelve concrete gravity dam models were created in order to get more reliable results. The structural model's attributes were developed using Latin Hypercube Sampling (LHS) technique. In this method, the probability distribution of each variable is divided into equal areas (a total of 12 areas for each random variable), and the numbers are randomly selected from each interval based on their distribution type. The lower and upper bounds of normal distribution were truncated at  $\mu - 5\sigma$  and  $\mu + 5\sigma$  to avoid the inclusion of physically unrealistic input data that could produce erroneous results. Conversely, the numbers are randomly generated from the whole area under the probability density function in the Monte Carlo Simulation (MCS) method. Consequently, MCS may not produce realistic results when the number of generated variates is low because it is possible that the majority or all numbers might be randomly selected from a certain range, which is addressed by increasing the number of models to obtain reliable results. To improve the accuracy of MCS, thousands or tens of thousands of simulations is needed (Nowak and Collins

Table 3 Random variates considered in this study

Model #	$E_c$ (GPa)	$f_c'$ (MPa)	$E_f$ (GPa)	$c$ (MPa)	$\mu$ (°)	$D$ (%)	$\alpha$	$\beta$
1	21.06	19.91	28.06	0.396	36.32	75	1.857	0.00352
2	21.93	22.48	14.47	0.363	37.67	09	1.587	0.00352
3	21.72	21.59	27.66	0.38	39.90	85	2.021	0.00393
4	17.47	18.36	16.18	0.333	43.59	32	1.831	0.00358
5	23.04	22.99	23.04	0.368	37.05	18	1.767	0.00365
6	26.96	27.65	20.47	0.336	41.51	93	1.905	0.00386
7	24.12	23.38	19.99	0.300	43.32	74	1.873	0.00340
8	20.43	20.27	22.12	0.389	44.27	54	2.064	0.00326
9	23.73	21.33	25.91	0.312	38.69	40	1.783	0.00371
10	19.55	22.14	25.08	0.321	35.02	47	1.977	0.00387
11	24.74	23.93	24.18	0.356	40.56	66	1.960	0.00378
12	22.60	25.22	18.60	0.345	41.67	05	2.044	0.00337

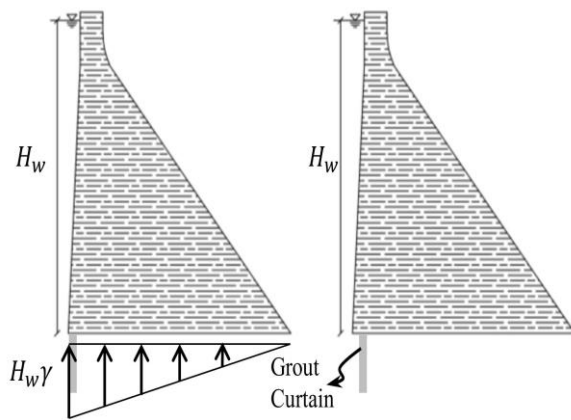


Fig. 4 Uplift pressure for 0 and 100% drain efficiency

2000). Therefore, MCS was deemed cost prohibitive for nonlinear seismic simulations of the scale used in this study. Hence, the Latin Hypercube Sampling method has an advantage over Monte Carlo Simulation method because it requires less computational effort, which is extremely important for complex problems such as the seismic response of concrete gravity dams. After obtaining random values for each random variable, they were randomly paired and the 12 models were created on ANSYS.

#### 4.3 Limit States (LS)

In this study, the following failure mechanisms are considered:

- Base Sliding (LS1)
- Cracking at the upstream face of the dam (LS2)
- Cracking at the neck of the dam (LS3)
- Excessive deformation (relative deformation) (LS4)

They are labeled (between parentheses) by the limit state function designation that will be used in this paper and are described in detail next.

##### 4.3.1 LS1: Base sliding

The sliding failure is the first failure mode considered in this study. Sliding stability has to be evaluated in safety analysis of concrete gravity dams. The contact surface of the dam-foundation rock is assumed to be horizontal, and is

Table 4 Expected damage level for different sliding thresholds

Sliding (cm)	Damage Level	References
2.5	Moderate	(Bernier <i>et al.</i> 2016)
5.0	Extensive	(Chavez and Fenves 1995)
15.0	Major	(Tekie and Ellingwood 2003)

modeled based on Mohr-Coulomb friction law. The friction angle and the cohesion of the contact are assumed to be equal to those of foundation rock.

The sliding limit state is checked in terms of maximum sliding displacement. In order to assess the sliding limit states, the three different limit states presented in Table 4 are considered based on published studies (Bernier *et al.* 2016, Tekie and Ellingwood 2003). Drain system damage is considered one of the consequences of sliding because the damage of the drain system can cause an increase in the effective uplift pressure level. Firstly, 2.5 cm is used to evaluate slight or minor drain system damage (Bernier *et al.* 2016). Secondly, 5 cm sliding displacement is used to evaluate maximum allowable sliding displacement of dams. This level of sliding can completely cause severe damage (Chavez and Fenves 1995). Thirdly, 15 cm (6 in.) is considered as unacceptable damage level for differential movements, which can cause loss of reservoir (Tekie and Ellingwood 2003). Based on these assumed sliding thresholds, the following three limit state functions are established. Three fragility curves are obtained based on these limit states.

$$LS1 - a : g(\delta_x) = \delta_x - 2.5 \text{ (cm)} \quad (7a)$$

$$LS1 - b : g(\delta_x) = \delta_x - 5.0 \text{ (cm)} \quad (7b)$$

$$LS1 - c : g(\delta_x) = \delta_x - 15.0 \text{ (cm)} \quad (7c)$$

##### 4.3.2 LS2: Tensile cracking at the upstream face of the dam

Cracking can have dire consequences in fluid retaining structures, especially plain concrete structures. In previous studies, crack formation due to tensile stresses at the upstream face of the dam was investigated in terms of maximum principal stress,  $\sigma_1$ , (see Fig. 5(a)) at any time during a seismic event. In this study, we introduce the effect of minimum principal stress  $\sigma_2$ . Kupfer *et al.* (1969) developed one of the first failure envelopes for concrete under a biaxial state of stress. It is known that in a multiaxial stress state, a state of biaxial or triaxial compression can lead to higher concrete strength than is observed under a uniaxial state of stress. This has led to a lot of research on the effects of confinement on concrete structures (Cho and Hall 2014, Liang and Sritharan 2018, Vu *et al.* 2009). It is also known that compressive stresses can reduce the tensile strength of concrete. Therefore, the tensile strength of concrete was taken as a function of the compressive strength of concrete and the corresponding compressive stress at any location. The resistance model for the principal tensile strength is determined as a function of the concrete capacity under uniaxial tension, using Eq. (8a).

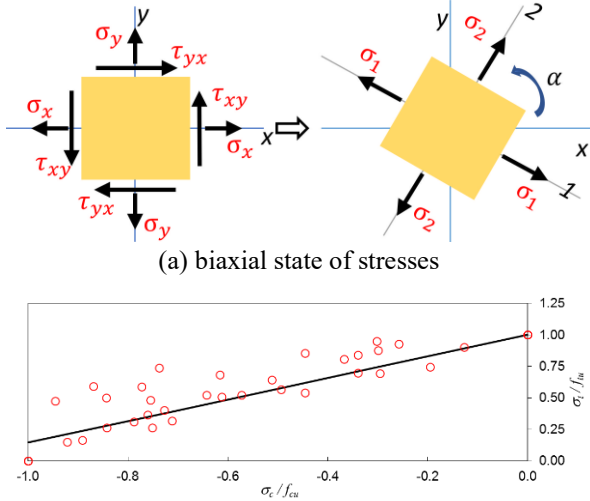


Fig. 5 State of stresses and failure envelope.

For the biaxial compression-tension state of stress, Eq. (8b) (Okeil 2006) is used, which is based on calibration of experimental data published in the literature for the compression-tension stress state as can be seen in Fig. 5(b).

$$f_{tu} = 0.30(f'_c)^{0.69} \text{ (MPa)} \quad (8a)$$

$$\sigma_{tu} = 0.30(f'_c)^{0.69} \times \left(1 + 0.85 \frac{\sigma_{cu}}{f'_c}\right) \text{ (MPa)} \quad (8b)$$

where  $f'_c$  is the compressive strength of concrete,  $f_{tu}$  is the tensile strength of uniaxially loaded concrete,  $\sigma_{tu}$  is the modified tensile strength of concrete accounting for the corresponding compressive stress, and  $\sigma_{cu}$  refers to the corresponding minimum principal stress. According to this failure model, concrete cracking occurs when the max principal stress exceeds the tensile strength,  $\sigma_{tu}$ , which can be significantly lower than the uniaxial tensile strength,  $f_{tu}$ . The fragility curve is obtained based on limit state function in Equation 9 which includes the effect of the biaxial state of stress considering the minimum principal stress.

$$\begin{aligned} LS2 : g(\ ) &= \sigma_1^{max} - \sigma_{tu} \\ &= \sigma_1^{max} - 0.30(f'_c)^{0.69} \times \left(1 + 0.85 \frac{\sigma_{cu}}{f'_c}\right) \text{ (MPa)} \end{aligned} \quad (9)$$

#### 4.3.3 LS3: Tensile cracking at the neck of the dam

Preliminary analyses results showed that the tensile stress around the neck can be significant. Therefore, the material failure around the neck of the dam was also checked in terms of maximum principal stresses using Eq. (8b). The fragility curve is obtained based on limit state function in Eq. (10).

$$LS3 : g(\ ) = \sigma_1^{max} - \sigma_{tu} \quad (10)$$

#### 4.3.4 LS4: Excessive deformation

Finally, excessive deformation of the dam body was checked in terms of relative deformation between the crest

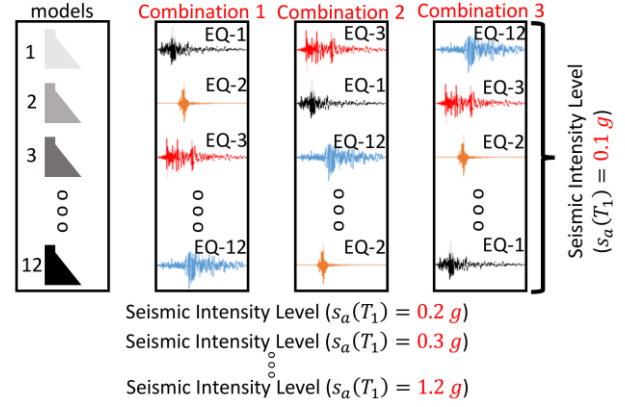


Fig. 6 Combination of ground motion and model uncertainties

and base. Excessive deformation of the dam body can impair the internal drainage system or cause service limitation for equipment. In the study, the difference between the horizontal displacements of crest and dam bottom is considered. The fragility curves are obtained based on the 1.71 cm and 3.42 cm relative displacements, which correspond to 0.014% and 0.028% of the dam height, respectively (Tekie and Ellingwood 2003). Based on these assumed relative deformation thresholds, the following two limit state functions are established. Two fragility curves are obtained based on these limit states.

$$LS4 - a : g(\ ) = (\delta_x^{top} - \delta_x^{bottom}) - 1.71 \text{ (cm)} \quad (11a)$$

$$LS4 - b : g(\ ) = (\delta_x^{top} - \delta_x^{bottom}) - 3.42 \text{ (cm)} \quad (11b)$$

## 5. Dynamic analyses

The fragility curves can be developed for different intensity measures such as the peak ground acceleration (PGA) or the spectral acceleration ( $S_a$ ) of the earthquakes (De Biasio *et al.* 2015). In this study, fragility curves are calculated as a function of  $S_a(T_1)$ , where  $T_1$  is the fundamental period of the dam system. Each one of the 12 prepared dam-water-foundation models was randomly paired with the three different ground motions from the 12 selected ground motions (see Fig. 6). Dynamic analyses were performed for each combination of the earthquake ground motion and the model at each intensity level from 0.1 g to 1.2 g in 0.1 g increments. Thus, a total of 432 non-linear dynamic analyses were conducted in this study.

### 5.1 Ground motion selection

In order to present the uncertainty in ground motion, the target spectrum was obtained based on the probabilistic seismic hazard analysis of the structure's site. The uniform hazard response spectrum in Fig. 7 is obtained for Pine Flat Dam site by using an online tool provided by (USGS 2018). Also, the distance from the epicenter of earthquake R and the magnitude of earthquake ( $M$ ) were selected based on

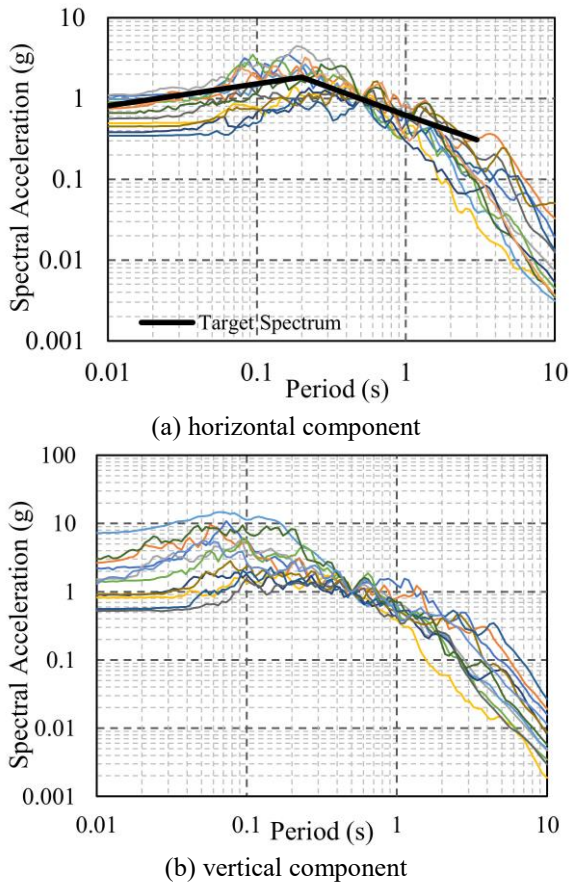


Fig. 7 Response spectra of the selected ground motions

deaggregation of the seismic hazard at the site

$$R = 0 - 50 \text{ km} \quad (12a)$$

$$M = 5.0 - 7.5 \quad (12b)$$

Based on these criteria, ground motions in Table 5 were selected from PEER Strong Ground Motion Data Base (PEER 2018). The response spectra of horizontal and vertical components of the selected ground motions are plotted in Fig. 7, respectively. All ground motions are scaled to 1.0 g at the fundamental period of the dam-reservoir-foundation rock system.

## 6. Results

### 6.1 Tornado diagrams

It was deemed necessary to first conduct a deterministic sensitivity analysis to evaluate the effect of the selected random variables on the sliding response, maximum principal stress at the upstream and the neck and excessive deformation. For each random variable, dynamic analyses were performed at the lower and upper bound of each random variable by considering the other random variables at their mean values. In tornado diagrams, the difference between the results of lower and upper boundaries is called a swing. The swing length shows the effect of variable. The

swing having the largest length is located at the top, and other swings follow it in a descending order. The median results are obtained by considering all random variables at their mean values. The results are normalized to 1.0 by dividing by the median results. Therefore, tornado diagrams show the ratio of variation. The horizontal and vertical components of Parkfield earthquake were selected for this study. The horizontal component of the earthquake is scaled to 0.4g peak PGA, which is a typical value for moderate to strong earthquakes (Chavez and Fenves 1995).

The sliding response results from the deterministic sensitivity analyses are presented in Fig. 8(a). It was found that the variability of the friction coefficient of the dam-foundation rock interface, drain efficiency and the elasticity modulus of the foundation rock have a significant impact on the sliding response of the dam. Also, the sliding response of the dam is less sensitive to damping and the elasticity modulus of the concrete. Chavez and Fenves (1995) showed that the sliding response of the dam increases when the ratio of the elasticity modulus of foundation rock to that of the concrete dam ( $E_f / E_c$ ) and the friction coefficient of interface increase. Therefore, the results presented in this study are consistent with the reported findings. Fig. 8(b) and Fig. 8(c) show the effects of the uncertainty parameters on the maximum principal stress of the upstream face and the neck of the dam, respectively. It is found that the elasticity modulus of the concrete, the damping, the friction coefficient of the dam-foundation rock interface and drain efficiency have a significant effect. However, the elasticity modulus of the foundation rock and cohesion parameters are less significant to maximum principal stress at the upstream face and the neck of the dam. Lastly, Fig. 8(d) shows the effects of the uncertainty parameters on the excessive deformation of the dam.

Consequently, all random variables except the cohesion of dam-foundation interface have an important effect on the limit state functions. However, the cohesion of the dam-foundation rock interface is less sensitive for all limit state functions. Nonetheless, all random variables were included in the reliability analyses reported herein.

### 6.2 Fragility curves

The results of the nonlinear analyses are used to estimate the fragility curves for the aforementioned limit states. Normal, Log-Normal and Weibull cumulative distribution types are compared to find the best fitting curve for the computed  $P_f$  result, which is defined as the number of failed simulations,  $N_f$ , divided by the total number of simulations,  $N$ .

$$P_f = \frac{N_f}{N} \quad (13)$$

The coefficient of determination  $R^2$  and root mean square error (RMSE) are considered as goodness-of-fit measures. The best fitting curve should have a higher value of the  $R^2$  and a lower RMSE value. The functions for Normal, Log-Normal and Weibull cumulative distribution are given by Eqs. (14), (15) and (16), respectively

$$F_x(S_a) = \Phi \left[ \frac{S_a - \mu}{\sigma} \right] \quad (14)$$

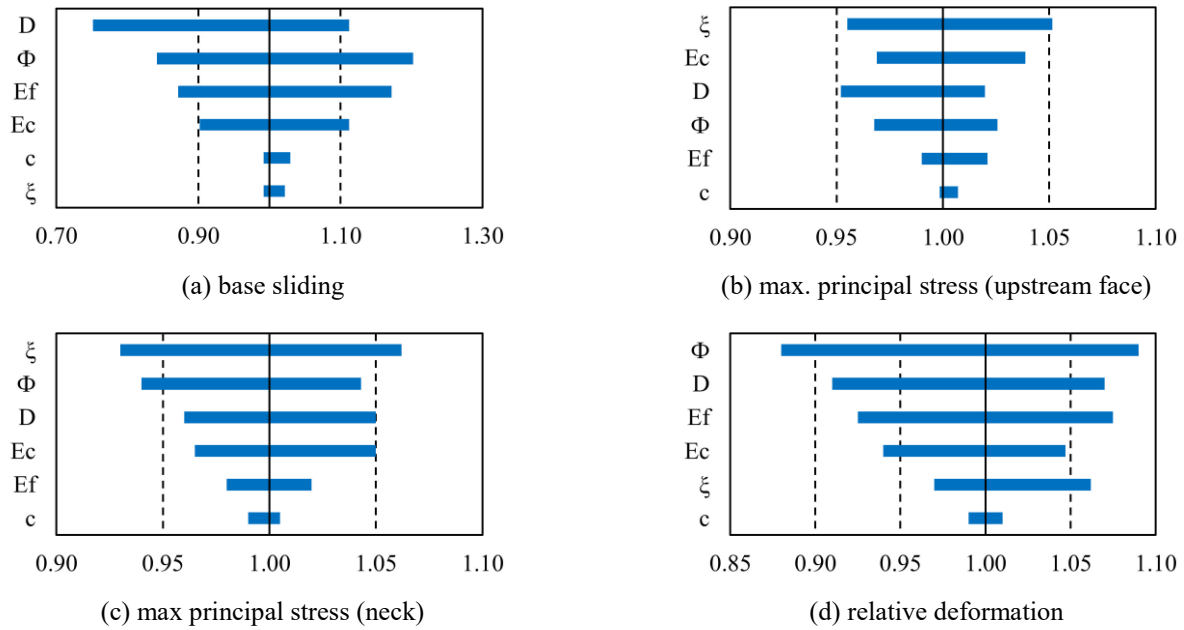


Fig. 8 Tornado diagrams

Table 5 Selected ground motions

#	Year	Event	Station	Mw	R (km)
1	1966	Parkfield	Cholame Shandon Array-8	6.19	12.9
2	1971	San Fernando	LA - Hollywood Stor FF	6.61	22.77
3	1978	Tabas, Iran	Boshrooyeh	7.35	24.07
4	1979	Coyote Lake	Gilroy Array #4	5.74	4.79
5	1980	Irpinia, Italy	Auletta	6.9	9.5
6	1980	Victoria, Mexico	Chichuachua	6.33	18.53
7	1980	Mammoth Lakes-01	Convict Creek	6.06	1.1
8	1983	Coalinga-05	Burnett Construction	5.77	8.3
9	1984	Morgan Hill	Gilroy Array #2	6.19	13.7
10	1986	N. Palm Springs	Sunnymead	6.06	37.9
11	1989	Loma Prieta	Capitola	6.93	8.65
12	1994	Northridge	Burbank - Howard Rd	6.69	16.9

where  $\Phi$  is standard normal cumulative distribution function,  $\mu$  is the mean value and  $\sigma$  is the standard deviation of the normal distribution, respectively.

$$F_x(S_a) = \Phi \left[ \frac{\ln(S_a/\mu)}{\sigma} \right] \quad (15)$$

where  $\mu$  is the mean value of the Log-Normal distribution, and  $\sigma$  is the logarithmic standard deviation.

$$F_x(S_a) = 1 - e^{-\left(\frac{S_a}{\alpha}\right)^\gamma} \quad (16)$$

where  $\alpha$  and  $\gamma$  are the shape and scale parameters of a Weibull distribution.

The results showed that the Log-Normal distribution has higher R2 and lower RMSE values compared to Normal and Weibull distribution for base sliding (LS1) and excessive deformation (LS4) limit states. Therefore, the Log-Normal distribution was considered to be the best fit for the sliding and excessive deformation limit state functions for the Pine Flat Dam. However, Weibull

distribution has the best fit for the tensile cracking at the upstream face (LS2) and neck of the dam (LS3) limit states. Table 6 lists the parameters of Normal, Log-Normal, and Weibull distributions. The fragility curves for the best fit are presented in Fig. 9 through Fig. 11.

### 6.3 Kolmogorov-Smirnov (K-S) Test

The Chi-Square and the Kolmogorov-Smirnov tests are the most commonly used methods to decide whether the assumed distribution type is acceptable or not (Haldar and Mahadevan 2000). The Chi-Square test is based on the error between the observed and assumed probability density function (PDF), while the Kolmogorov-Smirnov test is based on the cumulative distribution function (CDF). Since fragility curves are CDFs, the Kolmogorov-Smirnov test is used in this study.

Kolmogorov-Smirnov test compares the observed cumulative frequency and the CDF of an assumed theoretical distribution. After arranging the observed data in

Table 6 Distribution parameters for LS1, LS2 LS3 and LS4

Distribution		LS1-a	LS1-b	LS1-c	LS2	LS3	LS4-a	LS4-b
Normal	$\mu$	0.620	0.914	1.529	0.521	0.339	0.164	0.369
	$\sigma$	0.221	0.269	0.270	0.190	0.152	0.072	0.074
Log-Normal	$\mu$	0.604	0.898	1.626	0.507	0.326	0.153	0.365
	$\sigma$	0.356	0.314	0.249	0.357	0.424	0.456	0.204
Weibull	$\gamma$	3.088	3.774	8.351	3.046	2.560	2.518	5.849
	$\alpha$	0.697	1.011	1.549	0.586	0.387	0.187	0.396

increasing order and corresponding theoretical data, the maximum difference between the observed cumulative frequency and the CDF of assumed theoretical distribution is estimated as

$$D_n = \max|F_X(x_i) - S_n(x_i)| \tag{17}$$

where  $F_X(x_i)$  is the theoretical CDF of assumed distribution and  $S_n(x_i)$  is the corresponding stepwise CDF of the observed ordered samples, and  $n$  is the sample size, which is 12 in this study. If the maximum difference,  $D_n$  is less than or equal to the  $D_n^\alpha$ , which is a tabulated value for a target significance level,  $\alpha$ , the assumed distribution be accepted at the significance level  $\alpha$

$$P(D_n \leq D_n^\alpha) = 1 - \alpha \tag{18}$$

In this study,  $\alpha = 5\%$  is significance level is used and the corresponding  $D_{12}^{0.05} = 0.3754$ . The test results are given in Table 7 for each distribution type. The  $D_n$  values were found to be lower than 0.3754 with the maximum value being 0.10. Hence, the Normal, Log-Normal, and Weibull distributions are all acceptable with the significance level 5% for the K-S test (Sen 2018).

**7. Discussions**

The summary of results for each limit state is given in Table 8. The  $S_a$  at 5% probability of failure and the probability of failure of limit state at 1.0 g spectral acceleration are presented. The base sliding displacement (LS1) and excessive deformation (LS4) results are given based on Log-Normal distribution results. However, the tensile cracking (LS2 and LS3) results are presented based on Weibull distribution results. The 5% probability of failure is common in civil engineering to check the safety of structures.

Tornado diagrams show that the contact surface friction angle of and drain efficiency have an important effect on all limit states. The damping of the system has a significant effect only principal stresses at the neck and the upstream face of the dam. However, the cohesion of the dam-foundation interface is found to be insignificant.

Base sliding fragility curves show that the probability of 5 cm sliding displacement, which is assumed to be the maximum allowable sliding displacement for dams, was found to be critical for an earthquake with  $S_a(T_1) = 1.0 g$ . The loss of reservoir control (LS1-c) is unlikely for a moderate to strong earthquakes.

The results from dynamic analyses showed the maximum principal stresses at the upstream face of the dam

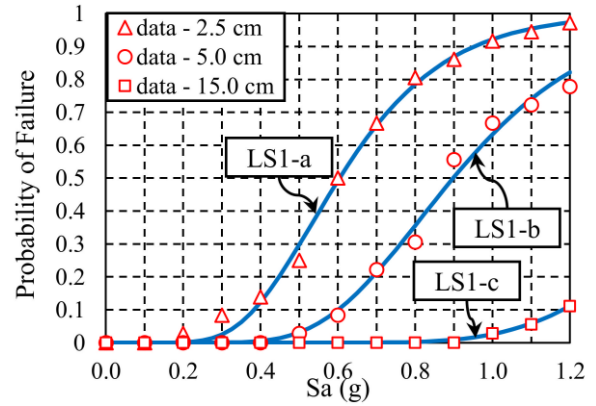


Fig. 9 Base sliding fragility curves (LS1)

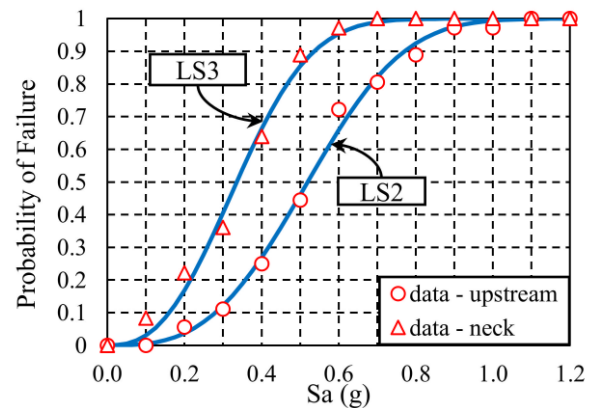


Fig. 10 Tensile cracking fragility curves (LS2 and LS3)

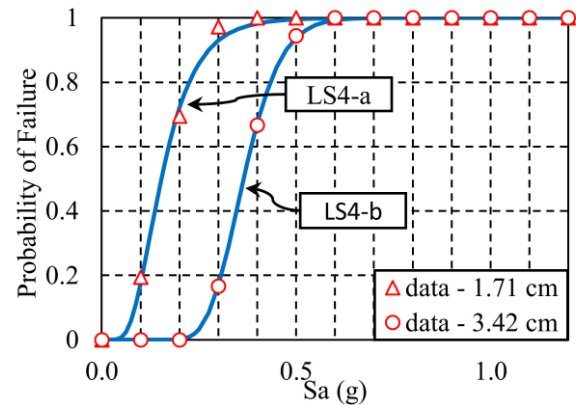


Fig. 11 Excessive deformation fragility curves (LS4)

occurred in the vicinity of the neck of the dam. It was also found that the maximum principal stresses at the neck of the dam occurred at the downstream face of the dam. The minimum principal stresses corresponding to the maximum principal stress are about 0 - 0.5 MPa. Due to this low level of minimum stresses, the effect of minimum principal stress on the tensile cracking capacity is insignificant. The tensile cracking around the neck was found to be more critical than the tensile cracking at other locations the upstream face.

Finally, the probability of excessive deformation of the dam was found to be significant compared to other limit states. This serviceability limit state is important because excessive deformations could impair the internal drainage

Table 7 Goodness-of-fit measure values for LS1, LS2, LS3 and LS4

Limit States	Normal		Log-Normal		Weibull	
	R <sup>2</sup>	RSME	R <sup>2</sup>	RSME	R <sup>2</sup>	RSME
LS1-a	0.995	0.031	0.996	0.026	0.994	0.031
LS1-b	0.983	0.043	0.992	0.029	0.981	0.044
LS1-c	0.989	0.004	0.992	0.003	0.987	0.004
LS2	0.997	0.026	0.996	0.029	0.997	0.025
LS3	0.995	0.029	0.986	0.049	0.996	0.022
LS4-a	1.000	0.004	0.998	0.017	1.000	0.003
LS4-b	1.000	0.008	1.000	0.003	0.999	0.014

Table 8 Summary of results

Limit State (LS)	$S_a$ at 5% probability (g)	Probability at 1.0g $S_a$ (%)
LS1-a 2.5 cm	0.34	92.19
LS1-b 5.0 cm	0.54	63.68
LS1-c 15.0 cm	1.08	2.55
LS2	0.22	99.38
LS3	0.12	100.00
LS4-a 1.71 cm	0.07	100.00
LS4-b 3.42 cm	0.26	100.00

system or cause service limitation for equipment.

## 8. Conclusions

Fragility curves are an important tool for evaluating the hazard levels and making structural risk assessments of infrastructure assets. They provide information about the vulnerability of structures corresponding to given demand levels. In this study, the fragility curves are calculated for a specific dam as a case study to demonstrate the methodology adopted in this research. Hence, the presented information is exclusively about the vulnerability of the dam chosen for the case study. The Latin Hypercube Sampling method is used as a practical and efficient way to evaluate structural uncertainties in lieu of the more demanding Monte Carlo Simulation method whose computational cost is prohibitive given the complexity of the problem and available resources. The earthquake ground motion data used in this study are obtained based on the target spectrum of Pine Flat Dam site. Non-linear dynamic analyses are performed by considering the effects of dam-reservoir-foundation rock interactions considering flexible foundation effects, compressible water, and absorptive reservoir bottom materials.

The following conclusions can be drawn from this study:

- The effect of minimum principal stresses on the tensile cracking capacity of the dam is low, at about 1-2%, due to the low principal stresses, which is about 0 – 0.5 MPa, when the maximum principal stress is maximum. Hence, this effect can be neglected in future studies.
- The Log-Normal distribution type is the most suitable distribution for the base sliding and excessive deformation fragility curves. The Weibull distribution type is the most suitable distribution for tensile cracking fragility curves.

- The maximum principal stresses at the neck of the dam occurred at the downstream face of the dam in the vicinity of the neck. The minimum principal stresses corresponding to the maximum principal stress are low and their effect on the tensile cracking capacity is insignificant.

- The tensile cracking probability of failure is more probable than the sliding of the dam. The 5% probability of failure of tensile cracking (LS3) is at 0.12 g spectral acceleration whereas that of 2.5 cm base sliding is at 0.34 g spectral acceleration.

- The probability of failure for base sliding (LS1-b) and tensile cracking (LS3) at 1.0g spectral acceleration are calculated 63.68% and 100.00%, respectively.

- While a base sliding of 5 cm, which is assumed to be the maximum allowable sliding displacement for dams, was found to be critical for an earthquake with  $S_a(T_1) = 1.0 g$ , the loss of reservoir control, which is estimated to happen at 15 cm base sliding, is unlikely for a moderate to strong earthquakes.

- The tensile cracking at the neck of the dam is found to be the most critical limit state with 100.00% probability of failure at 1.0 g spectral acceleration.

- The probability of excessive deformation of the dam, which can impair the internal drainage system or cause service limitation for equipment, is found to be significant compared to other limit states.

It should be noted that while the aforementioned conclusions are specific to the Pine Flat Dam, the methodology is applicable to other concrete gravity dams.

## Acknowledgments

The authors would like to acknowledge the financial support provided to the first author by the General Directorate of State Hydraulic Works, The Republic of Turkey, to pursue his graduate studies in the United States. Additional support from the Department of Civil and Environmental Engineering at Louisiana State University is also acknowledged. Any opinions, findings, and conclusions or recommendations expressed in this material are those of the authors and do not necessarily reflect the views of the sponsoring agencies.

## References

- ACI (2014). "Building Code Requirements for Structural Concrete and Commentary (ACI 318-14)", 317.
- ANSYS (2018), Theory Reference Manual, version 18.2, Canonsburg, P.A. U.S.A.
- ASCE (2017), "2017 Report Card for America's Infrastructure: Dams", American Society of Civil Engineers.
- Bernier, C., Padgett, J.E., Proulx, J., and Paultre, P. (2016), "Seismic fragility of concrete gravity dams with spatial variation of angle of friction: case study", *J. Struct. Eng.*, **142**(5), 05015002. [https://doi.org/10.1061/\(ASCE\)ST.1943-541X.0001441](https://doi.org/10.1061/(ASCE)ST.1943-541X.0001441).
- Chavez, J.W., and Fenves, G.L. (1995). "Earthquake analysis of concrete gravity dams including base sliding", *Earthq. Eng.*

- Struct. Dyn.*, **24**(5), 673-686.  
<https://doi.org/10.1002/eqe.4290240505>.
- Cho, I.H. and Hall, J.F. (2014), "General confinement model based on nonlocal information", *J. Eng. Mech.*, **140**(6), 17.  
<https://doi.org/10.1002/eqe.4290240505>.
- De Araujo, J.M. and Awruch, A.M. (1998), "Probabilistic finite element analysis of concrete gravity dams", *Advan. Eng. Soft.*, **29**(2), 97-104. [https://doi.org/10.1016/S0965-9978\(98\)00052-0](https://doi.org/10.1016/S0965-9978(98)00052-0).
- De Biasio, M., Grange, S., Dufour, F., Allain, F. and Petre-Lazar, I. (2015), "Intensity measures for probabilistic assessment of non-structural components acceleration demand", *Earthq. Eng. Struct. Dyn.*, **44**(13), 2261-2280.  
<https://doi.org/10.1002/eqe.2582>.
- Ellingwood, B. and Tekie, P.B. (2001), "Fragility analysis of concrete gravity dams", *J. Infr. Sys.*, **7**(2), 41-48.  
[https://doi.org/10.1061/\(ASCE\)1076-0342\(2001\)7:2\(41\)](https://doi.org/10.1061/(ASCE)1076-0342(2001)7:2(41)).
- Fenves, G., and Chopra, A.K. (1984), "Earthquake analysis of concrete gravity dams including reservoir bottom absorption and dam water foundation rock interaction", *Earthq. Eng. Struct. Dyn.*, **12**(5), 663-680.  
<https://doi.org/10.1002/eqe.4290120507>.
- Fenves, G., and Chopra, A.K. (1987), "Simplified earthquake analysis of concrete gravity dams", *J. Struct. Eng.*, **113**(8), 1688-1708.  
[https://doi.org/10.1061/\(ASCE\)0733-9445\(1987\)113:8\(1688\)](https://doi.org/10.1061/(ASCE)0733-9445(1987)113:8(1688)).
- Ghanaat, Y., Patev, R.C. and Chudgar, A.K. (2012), "Seismic fragility analysis of concrete gravity dams", *15th World Conference on Earthquake Engineering*, Sociedade Portuguesa de Engenharia Sismica (SPES), Lisbon, Portugal.
- Goldgruber, M., Shahriari, S. and Zenz, G. (2015). "Dynamic sliding analysis of a gravity dam with fluid - structure-foundation interaction using finite elements and newmark's sliding block analysis", *Rock Mech. Rock Eng.*, **48**(6), 2405-2419. <https://doi.org/10.1007/s00603-015-0714-1>.
- Haldar, A. and Mahadevan, S. (2000), Probability, reliability and statistical methods in engineering design, John Wiley, New Jersey, U.S.A.
- Hariri-Ardebili, M.A., and Saouma, V.E. (2016a), "Collapse fragility curves for concrete dams: comprehensive study", *J. Struct. Eng.*, **142**(10), 04016075.  
[https://doi.org/10.1061/\(ASCE\)ST.1943-541X.0001541](https://doi.org/10.1061/(ASCE)ST.1943-541X.0001541).
- Hariri-Ardebili, M.A., and Saouma, V.E. (2016b), "Seismic fragility analysis of concrete dams: A state-of-the-art review", *Eng. Struct.*, **128**(1), 374-399.  
<https://doi.org/10.1016/j.engstruct.2016.09.034>.
- Hoek, E. and Brown, E.T. (1997), "Practical estimates of rock mass strength", *Int. J. Rock Mech. Min.*, **34**(8), 1165-1186.  
[https://doi.org/10.1016/S1365-1609\(97\)80069-X](https://doi.org/10.1016/S1365-1609(97)80069-X).
- Kupfer, H.B., Hilsdorf, H.K. and Rusch, H. (1969), "Behavior of concrete under biaxial stresses", *ACI J. Proceedings*, **6**(8), 656-666.
- Leger, P. and Boughoufalah, M. (1989), "Earthquake input mechanisms for time-domain analysis of dam-foundation systems", *Eng. Struct.*, **11**(1), 37-46.  
[https://doi.org/10.1016/0141-0296\(89\)90031-X](https://doi.org/10.1016/0141-0296(89)90031-X).
- Li, L.X. Li, H.N. and Li, C. (2018), "Seismic fragility assessment of self-centering RC frame structures considering maximum and residual deformations", *Struct. Eng. Mech.*, **68**(6), 677-689.  
<https://doi.org/10.12989/sem.2018.68.6.677>.
- Liang, X. and Sritharan, S. (2018), "Effects of confinement in circular hollow concrete columns", *J. Struct. Eng.*, **144**(9), 13, 04018159.
- Løkke, A., and Chopra, A. K. (2015). "Response Spectrum Analysis of Concrete Gravity Dams Including Dam-Water-Foundation Interaction." *J Struct Eng*, 141(8), 04014202.  
[https://doi.org/10.1061/\(ASCE\)ST.1943-541X.0002151](https://doi.org/10.1061/(ASCE)ST.1943-541X.0002151).
- Lupoi, A. and Callari, C. (2011), "A probabilistic method for the seismic assessment of existing concrete gravity dams", *Struct. Infr. Eng.*, **8**(10), 985-998.  
<https://doi.org/10.1080/15732479.2011.574819>.
- Moradloo, J., Naserasadi, K. and Zamani, H. (2018), "Seismic fragility evaluation of arch concrete dams through nonlinear incremental analysis using smeared crack model", *Struct. Eng. Mech.*, **68**(6), 747-760.  
<https://doi.org/10.12989/sem.2018.68.6.747>.
- Morales-Torres, A., Escuder-Bueno, I., Altarejos-García, L. and Serrano-Lombillo, A. (2016), "Building fragility curves of sliding failure of concrete gravity dams integrating natural and epistemic uncertainties", *Eng. Struct.*, **125**(15), 227-235.  
<https://doi.org/10.1016/j.engstruct.2016.07.006>.
- Nielson, B.G. and DesRoches, R. (2007), "Seismic fragility methodology for highway bridges using a component level approach", *Earthq. Eng. Struct. Dyn.*, **36**(6), 823-839.  
<https://doi.org/10.1002/eqe.655>.
- Nowak, A.S. and Collins, K.R. (2000), Reliability of Structures, McGraw Hill, U.S.A.
- Nowak, A.S. and Szerszen, M.M. (2003), "Calibration of design code for buildings (ACI 318): Part 1 - Statistical models for resistance", *ACI Struct. J.*, **100**(3), 377-382.
- Okeil, A. M. (2006). "Allowable tensile stress for webs of prestressed segmental concrete bridges." *ACI Struct J*, 103(4), 488-495.
- PEER (2018), "PEER Strong Ground Motion Database." Pacific Earthquake Engineering Research Center.
- Salimi, M.R. and Yazdani, A. (2018), "Reliability-based fragility analysis of nonlinear structures under the actions of random earthquake loads", *Struct. Eng. Mech.*, **66**(1), 75-84.  
<https://doi.org/10.12989/sem.2018.66.1.075>.
- Sen, U. (2018), "Risk Assessment of Concrete Gravity Dams under Earthquake Loads." M.S. Thesis, Department of Civil and Environmental Engineering, Louisiana State University, Louisiana, U.S.A.
- Tekie, B.P., and Ellingwood, B.R. (2003), "Seismic fragility assessment of concrete gravity dams", *Earthq. Eng. Struct. Dyn.*, **32**, 2221-2240. <https://doi.org/10.1002/eqe.325>.
- USACE (1995), Gravity Dam Design, US Army Corps of Engineers, Washington, D.C. U.S.A.
- USGS (2018), "Unified Hazard Tool", United States Geological Survey, Unified Hazard Tool.
- Vu, X.H., Malecot, Y., Daudeville, L. and Buzaud, E. (2009), "Experimental analysis of concrete behavior under high confinement: Effect of the saturation ratio", *Int. J. Solids Struct.*, **46**(5), 1105-1120.  
<https://doi.org/10.1016/j.ijsolstr.2008.10.015>.